JOURNAL OF MATERIALS SCIENCE 24 (1989) 3361–3370

TEM characterization of some crude or air heat-treated SiC Nicalon fibres

YVES MANIETTE, AGNÈS OBERLIN
Laboratoire Marcel Mathieu, UA 1205 C.N.R.S. Universite, 2 avenue du président Angot, F-64000 Pau, France

Commercial Nicalon fibres were prepared by thin transverse sectioning and studied by transmission electron microscopy. A progressive tilting of the incident beam allows us to explore the selected-area diffraction (SAD) pattern along two orthogonal directions, increasing the tilting angle (dark-field (DF) imaging). The lattice fringes technique was also used. The samples were Nicalon 001, 101 and 201 fibres, the latter also being studied after heat treatment in air at 1300° C for 48 h. The SAD pattern of the 001 fibre only shows the SiC_{111} intense halo whereas the other samples show all the SiC (1 1 1, 2 2 0 and 3 1 1) strongly scattered beams, indicating a microcrystalline state. Correspondingly, DF imaging does not indicate any localized measurable scattering domain for 001. Only bright dots can be seen, less than 1 nm in size. The other fibres show SiC microcrystals respectively 2 nm (1 0 1), 3 nm (2 0 1) and up to 7 nm (heat-treated 2 0 1) in extent. Free aromatic carbon, shaped in small units less than 1 nm in size fills up the interstices between SiC. These units tend to lie flat on SiC. In heat-treated fibres, they form incomplete layers around the edges. In addition, the heat-treated 2 0 1 fibre show a 1 μm thick layer of cristobalite at the fibre surface. These crystals are polytypes.

1. Introduction

Commercial SiC fibres are now often used in the processing of some composite materials. Their microstructure has already been studied by numerous techniques [1–6]. Indeed, the region very near the edge of the fibre plays an important part in the adhesion between the fibre and the matrix of a composite material. High-resolution transmission electron microscopy (TEM) provides us with a convenient tool in order to characterize the microstructure either inside the fibre or at its surface.

2. Techniques

2.1. Sample preparation

The TEM requires samples less than about 100 nm thick. Ultramicrotomy has been used in order to obtain such samples. A single filament is extracted from a yarn and embedded in an epoxy resin (Polarbed 812) and processed so as to achieve the greatest hardness. The sample is then thinly sliced with a microtome (L.K.B. Ultrotome V) equipped with a diamond knife (Diatome). The thickness of the sections is less than 100 nm and can be measured approximately by observing their colour [7]. The knife rate is 1 mm sec^{-1} during the sectioning operation.

It is not possible to obtain a perfect section from such a brittle material because the specimen tends to break in small particles less than 1 μm long, having some conchoidal fracture surfaces which are characteristic of a glass-like material. Fig. 1, which can be observed with a stereoscope, shows such particles; a conchoidal fracture surface can be noted on the upper particle. Some of the particles are still bonded with the embedding medium and can be characterized with certainty as being the external part of the fibre. It must be noticed that some areas of the fibre after having been broken are blown away by the diamond knife. However, if a sufficient number of sections is explored, areas can be found where the various eventually present phases are clearly attached to each other without being disturbed.

Ion-beam thinning was not employed, because of the risk of selective etching and to the amorphization phenomenon on the edges of the thin foils.

2.2. Electron microscopy (TEM)

2.2.1. Principles

In the electron microscope the specimen is placed beyond the object focal plane of the objective lens. The electron beam gives rise to a diffraction pattern in the image focal plane of this lens and to a magnified image of the object in the image plane. Projector lenses are then used for focusing either the diffraction pattern or the magnified image of the object on the photographic plate.

By placing an aperture (objective aperture) in the diffraction plane, it is possible to select one or several scattered beams for making a magnified image of the object. Three different techniques can be processed.

1. Bright field (BF): the aperture is placed on the optical axis of the microscope, at the centre of the diffraction pattern, so as to permit only the incident

0022–2461/89 $03.00 + .12

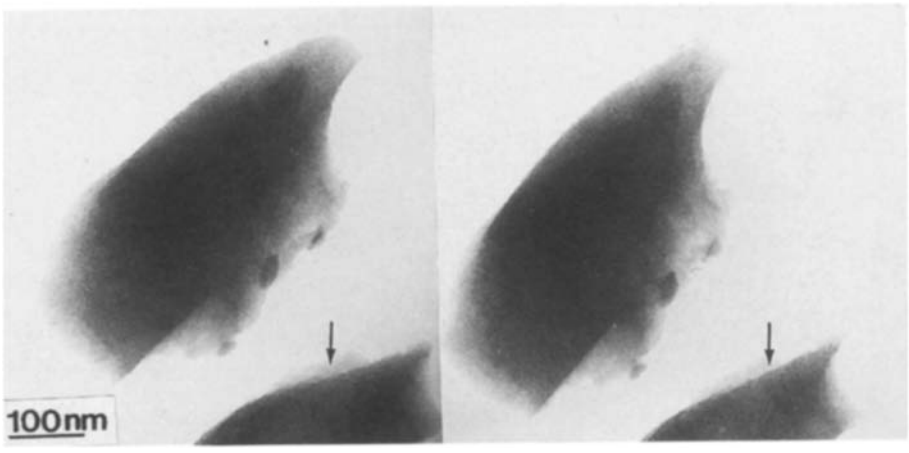

Figure 1 Stereomicrograph showing the representative shape of SiC particles cut with a diamond knife.

beam to pass through. In this way, crystals giving rise to strongly scattered beams withdrawn by the aperture will appear darker than the others. The image will result from an amplitude contrast.

2. Dark field (DF): the aperture is placed on the optical axis of the microscope, but the incident beam is tilted at a 2θ angle. This allows only the 2θ scattered beam to pass through the aperture. Scattering crystals will appear bright, on a dark background.

3. Lattice fringes (LF): a greater aperture is used, so as to allow two or more scattered beams to pass through it. The image will be made by the interference of these beams. If the object is thin enough, the image will be the result of a phase contrast.

By placing an aperture in the image plane, it is possible to select a part of the image, i.e. of the specimen, and to make its diffraction pattern. The selected-area diffraction technique (SAD) allows us to obtain the diffraction pattern of an area approximately 1 μm wide.

2.2.2. Exploration of the reciprocal space

Dark-field techniques can be used for determining both the nature, the size and the orientation in space of the components of a polyphasic material, even if it is complex or if some of the phases are in a very small amounts or if they are made of very small crystals [8–10]. Whatever its size, a crystal scatters characteristic $h\,k\,l$ beams: if one of them can be separated from all the others by using a suitable aperture, the crystal will appear as a small bright area on a dark field. Its spatial orientation will be determined if the aperture position in the selected-area diffraction pattern is known. The tilted incident beam can be displaced around a cone the half-summit angle of which is 2θ. In this way a given d_{hkl} Debye–Scherrer ring can be explored and any preferred orientation can be detected in the sample.

The size of a crystal recorded in this way will be measurable if it is larger than δ, the resolution being permitted by the aperture. In the present work the diameter of the aperture was $2\,nm^{-1}$, giving the result $\delta = 0.8$ nm. As an example, Fig. 2 shows the radial distribution of the SiC scattered beams in the selected-area diffraction pattern, in relation to the aperture size. If additional phases are present they will be identified if their scattered beams are localized in the empty areas of the SiC pattern: this is the case for aromatic turbostratic carbon (0 0 2 scattered beam) and SiO_2 more intensely scattered beams (Fig. 2).

Carbon and SiO_2 are mentioned here because they have already been observed in pyrolysed SiC fibre precursors [11] and SiC fibres [2, 3]. They are assumed to be present because of the elemental composition of the fibre, showing the presence of carbon and oxygen in excess. However, because of the aperture diameter (Fig. 2) it is not possible to separate the C_{002} and the SiO_2 scattered beams, and if there is any silica, it will be imaged with carbon. By increasing the tilt angle, SiC_{111} and C_{10} scattered beams will pass through the objective aperture. The corresponding crystals will be thus imaged altogether. An additional increase of the tilt angle will allow us to obtain images of SiC alone, using either 2 2 0 or 3 1 1 scattered beams.

3. Results

3.1. NLP 001 fibre

The selected-area diffraction pattern of this fibre (Fig. 3a) only shows continuous SiC haloes instead of sharp rings or arcs. There is thus no preferential orientation and the material could be amorphous.

The dark-field micrographs (Figs 4a and b) corresponding to a radial exploration of the selected-area diffraction pattern (see Fig. 2) show a homogeneous statistical distribution of bright dots, the size of which is given by the microscope resolution. Whatever the

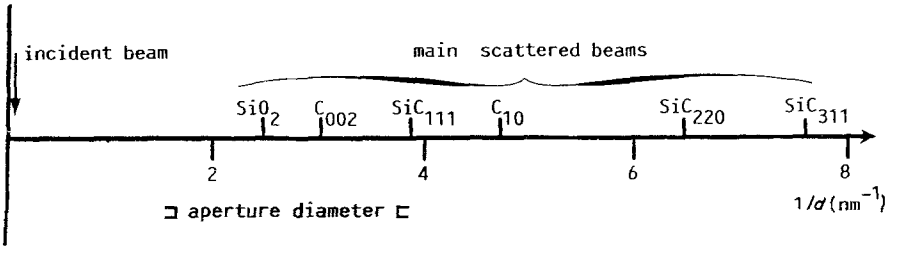

Figure 2 The main scattered beams to be expected from a SiC fibre, compared with the objective aperture size.

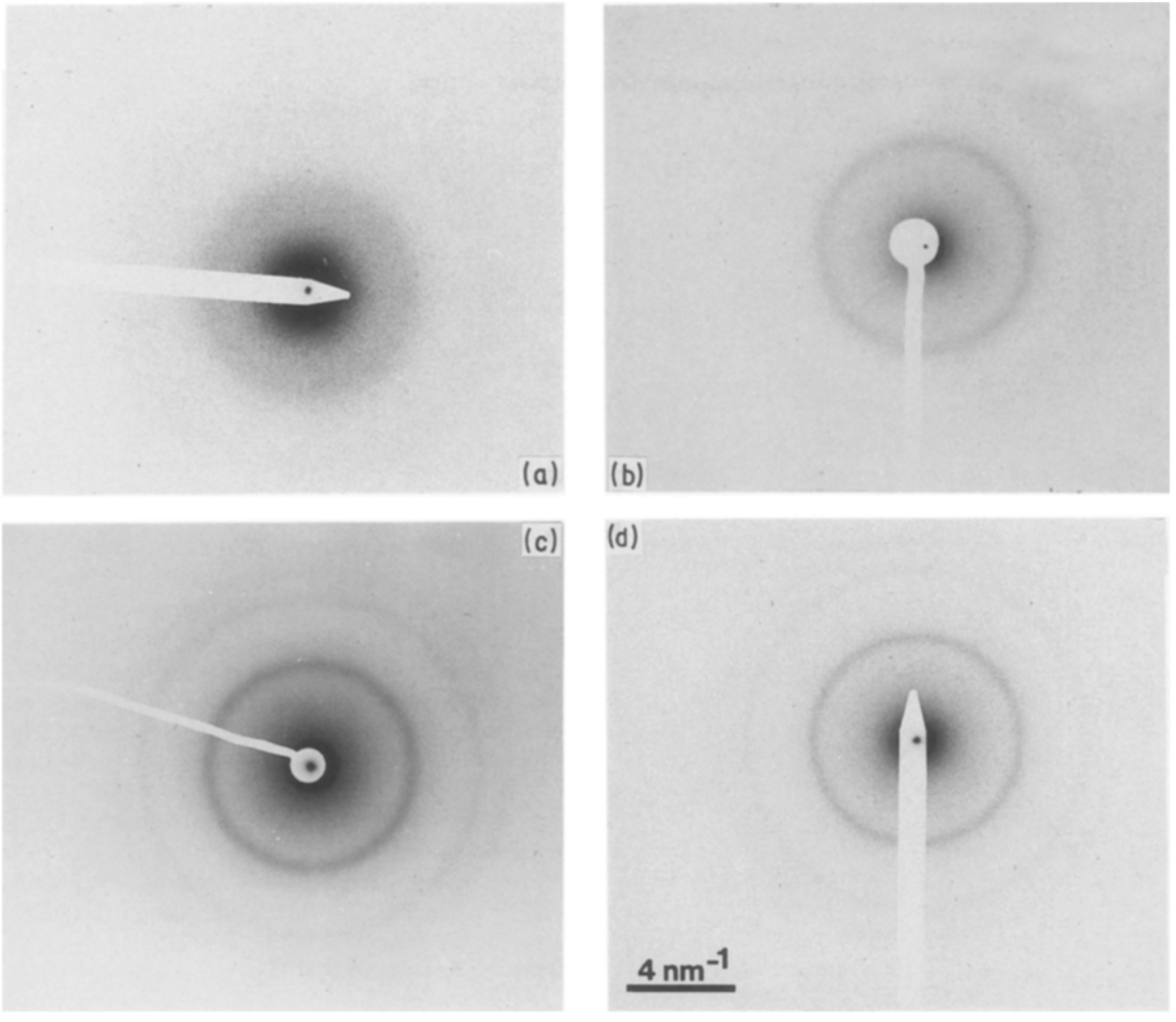

Figure 3 Selected-area diffraction patterns of the samples: (a) NLP 001; (b) NLP 101; (c) NLP 201; (d) heat-treated NLP 201.

position of the aperture, such bright dots can be observed and they always appear in focus. This kind of imaging is characteristic of an amorphous material [12]. The fibres are homogeneous from the surface to the centre, and no mixture of phases can be observed as localized areas in thin sections.

3.2. NLP 101 fibre

Fig. 3 shows the selected-area diffraction pattern of this fibre. Three Debye–Scherrer rings can be seen, corresponding to SiC_{111}, SiC_{220} and SiC_{311} scattered beams. It is hence possible to say that there is a three-dimensional order in SiC.

Figs 5a and b correspond to C_{002}–SiO_2 dark fields for two orthogonal positions of the aperture, whereas Fig. 5c corresponds to the SiC_{111} dark field. These micrographs have been recorded on a particle firmly attached to the embedding medium. They correspond thus to the fibre surface. The comparison between the micrographs first shows that a thin layer of constant thickness occupies the external edge of the fragment. This layer is about 20 nm thick and does not occur everywhere in the thin sections, but only in a few areas. It does not give any define contribution in any of the successive dark-field micrographs. However, the visual observation on the microscope screen shows very small bright domains the position and intensity of which change very fast when exposed to the incident beam. During the exposure time (a few seconds) all these moving individuals (Figs 5a, b) show that except on this 20 nm layer, the particle is formed of individual bright domains the size of which is similar to the resolving power of the microscope (0.8 nm). The comparison between Fig. 5a and Fig. 5b shows that a rim, brighter than the main part of the particle, is detected in (a) (arrow) and disappears in (b). The brightness of this rim is due to a higher density of individual domains in (a), relative to (b). This phenomenon suggests the occurrence of a preferred orientation of the individual domains along the edges of the particles. Such oriented rims entirely disappear in the SiC_{111} and SiC_{220} dark fields. Fig. 5c shows individual bright domains homogeneously distributed everywhere in the particle. Their sizes have been measured on the best focused micrographs and have been found to be, at most, 2 nm.

These data first suggest that three different phases are present near the fibre surface in the studied section. The first two phases, i.e. the 20 nm layer and the oriented rim, consist of SiO_2 and carbon, respectively; the third phase, which is the major component, consists of SiC and is to be found throughout the interior of the particle.

The layer is typically amorphous, and could thus be

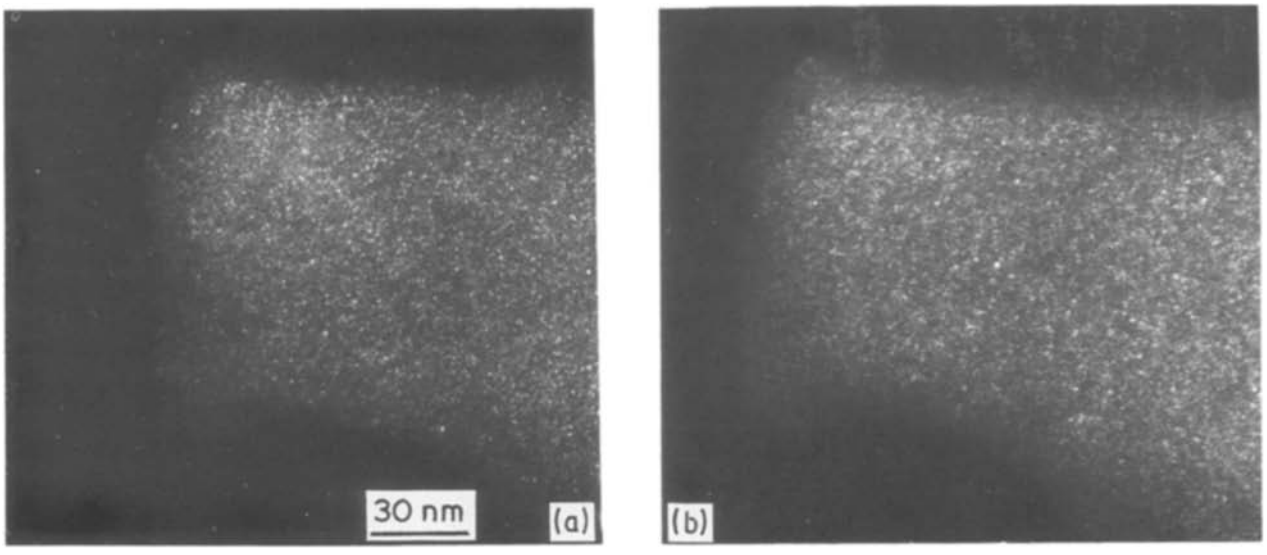

Figure 4 NLP 001 fibre. (a) C_{002} dark field; (b) SiC_{111} dark field.

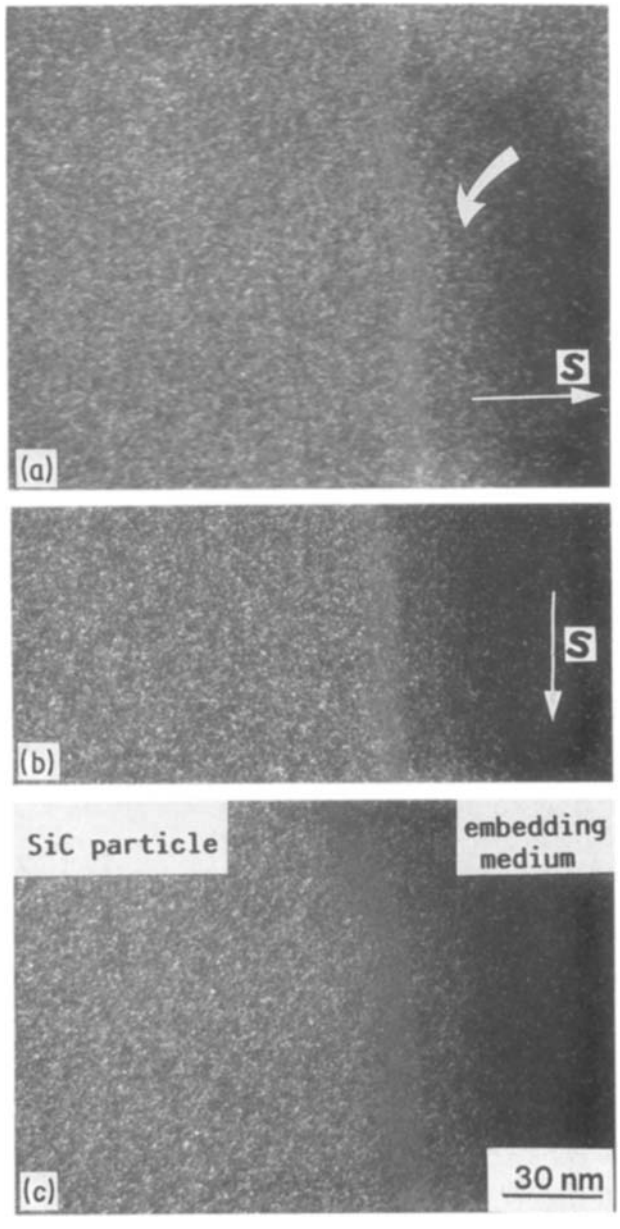

Figure 5 NLP 101 fibre, external part. The directions of the scattering vectors are shown. (a, b) C_{002} dark fields. (c) SiC_{111} dark field.

silica. The oriented rim cannot be amorphous, but is compatible with planar aromatic ring structures, either single or stacked in small numbers. Such structures are very common in carbonaceous materials at the start of the carbonization process [10] and are called basic structural units (BSU). Basic structural units were observed as having a strong tendency to lie flat on any substrate [13, 14], where they can easily appear as oriented rims when they are seen edge-on: the oriented rims could thus be attributed to turbostratic carbon. Because of the small amount of carbon and the fact that the structure factor of the C_{002} reflection is smaller than that of the SiC_{111} one, it is not possible to see any C_{002} diffraction ring or arc on the patterns.

If we add selected-area diffraction data (Fig. 3b) to SiC dark-field data (Fig. 5c), the SiC phase is undoubtedly crystallized, but the particle sizes are only just measurable. The crystal sizes in the bulk of the observed fragments are homogeneous.

Particles localized in the inner part of the fibre show the same features as those already described, except the amorphous silica layer which can never be observed. Thus, we can conclude that this layer is caused by a surface oxidation.

3.3. NPL 201 fibre

Fig. 3c is the selected-area diffraction pattern of this sample. The three SiC rings are sharper than for the former sample. It should be noted that as in the case of the other samples, no 0 0 2 ring of carbon can be detected.

Figs 6a and b show C_{002}–SiO_2 dark fields of a particle attached to the embedding medium, with the incident beam rotated 90° from (a) to (b), corresponding to two orthogonal positions of the aperture. As in Fig. 5, an oriented rim of bright domains appears, which we assume to be carbon. The size of the basic structural units is about the same as in Figs 5a and b, but they are brighter, indicating a better parallelism in the carbon layer stacks [8]. However, it must be noted

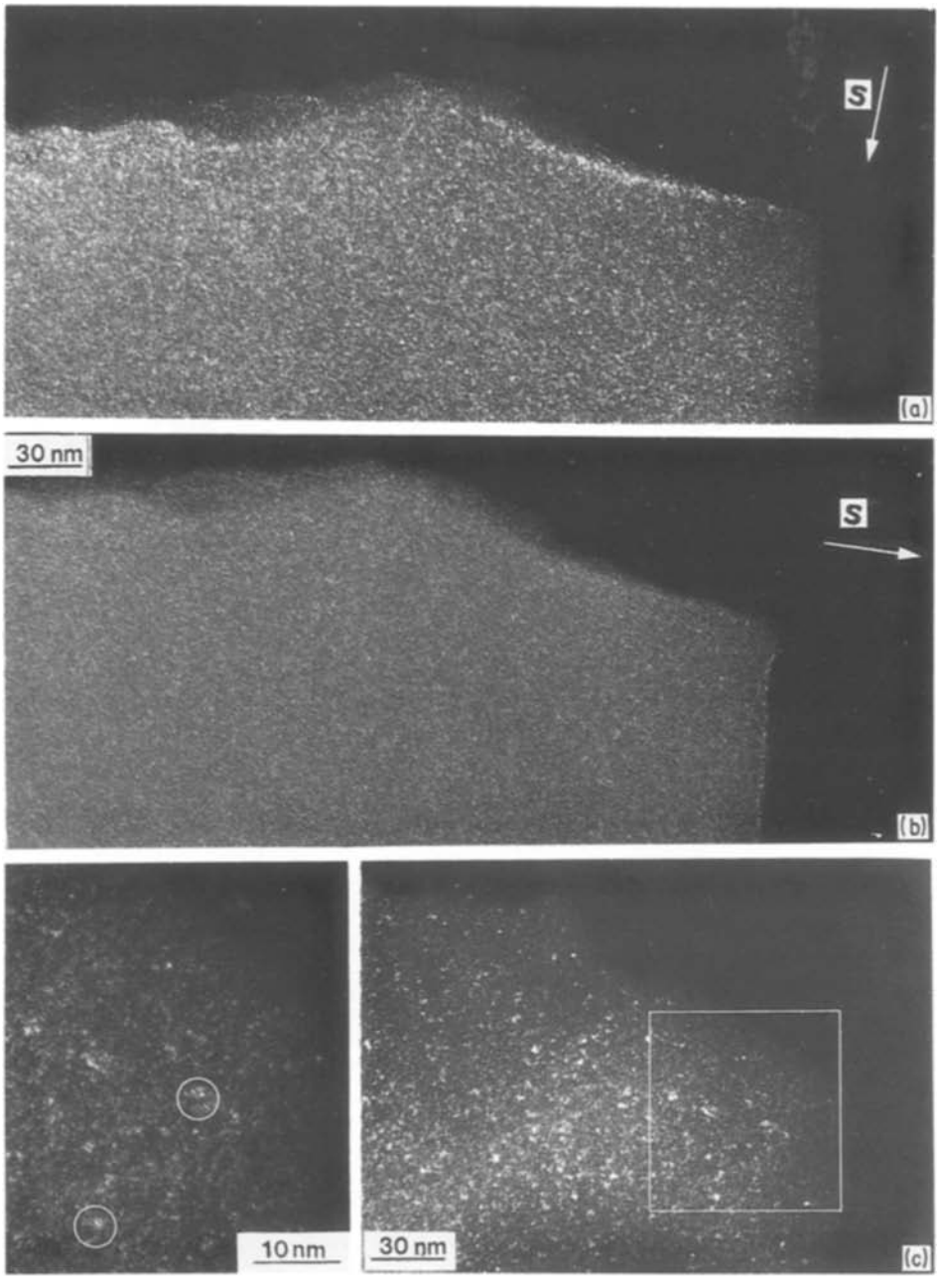

Figure 6 NLP 201 fibre. (a, b) C_{002} dark fields. (c) SiC_{111} dark field. Inset: higher magnification of (c), showing Moiré fringes inside SiC crystals.

that this oriented rim is parallel to the microtome knife edge: this will be discussed further. No amorphous layer could be detected in the thin sections. Fig. 6c corresponds to SiC_{111}. The basic structural units and oriented rim disappear. On the other hand, some larger SiC crystals can now be observed. In the largest ones (up to 3 nm), Bragg and Moiré fringes are visible (circles in the inset of Fig. 6c).

3.4. Heat-treated NLP 201 fibre

3.4.1. External phase

The low-magnification micrographs of the sections show a layer, about 1 μm thick, of a crystalline phase which is disturbed by the electron beam and becomes amorphous: in Fig. 7a diffraction extinction contours are shown, which promptly disappear when the particle is exposed to the electron beam. Many decohesions are observed, due to the poor adhesion between this layer and the fibre. Fig. 7c shows an area where the embedding medium has replaced a part of the layer, which has been chipped during a mechanical manipulation. This emphasizes the hypothesis of easy fracturation and allows us to suppose that cracks and decohesions are not artefacts of the preparation process.

It is possible, however, to record some selected-area diffraction patterns of this crystalline phase. This allows us to identify polycrystalline cristobalite on the surface of the fibre. The cubic crystals are often replaced by polytypes (Fig. 8a). During irradiation the cristobalite becomes amorphous and its 1 1 1 reflection (0.415 nm) is transformed into a faint and diffuse halo, the diameter of which corresponds to the same distance (Fig. 8b). When the amorphization has occurred, this diffuse halo is the only one to be observed on the selected-area diffraction pattern (Fig. 8c). This electron amorphized silica shows the same phenomenon already observed in Fig. 5 with regard to the 20 nm

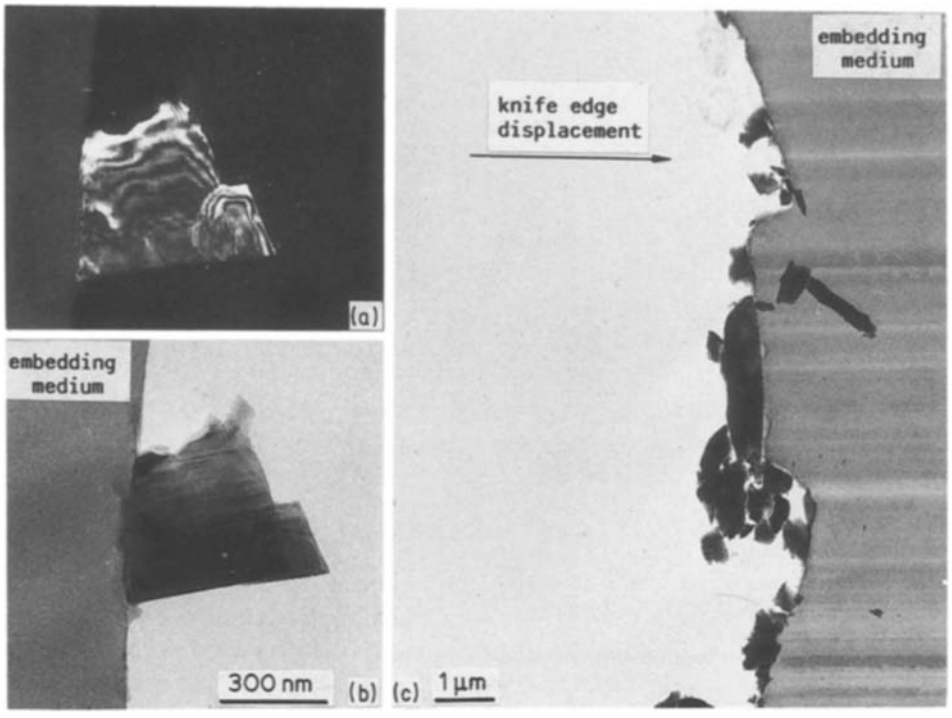

Figure 7 Heat-treated NLP 201 fibre. (a, b) Dark field and bright field of a cristobalite particle, showing diffraction extinction contours. (c) Bright field of a part of the section, showing the chipping phenomenon about the cristobalite layer.

layer on the NLP 101 fibre, and is an additional characterization parameter for identifying silica.

On the other hand, it must be noticed that large cristobalite crystals produced during the glass crystallization process are stable under the electron beam [15]. The lattice fringes technique applied to such samples allows us to record sequences which are typical of polytypism (Fig. 9).

3.4.2. Fibre

In the areas of the fibre centre, neither cristobalite nor amorphous silica can be observed, but only carbon and SiC crystals. Under the heat treatment, they undergo a major transformation, and there is a marked improvement in their organization. Figs 9a to c and 10a to c, respectively, show micrographs of two orthogonal C_{002} dark fields and a SiC_{111} dark field. The individual carbon BSU observed in the crude fibre are fused in continuous short bands, and can be recorded by means of the lattice fringes technique (Fig. 11) as continuous carbon layers. The SiC crystals (Fig. 10c) have greatly increased in size, now measuring up to 7 nm. Fig. 11 reveals an interesting phenomenon, already discussed in another paper [16]: the carbon layers form incomplete shells around each SiC crystal. In Fig. 11 these crystals are evinced by their 1 1 1 fringes (single arrows). The carbon shells forming some kind of nets are evinced by their 0 0 2 fringes (double arrows). The size of the SiC crystals measured by the lattice fringe technique agree well with dark-field technique data. The improvement in the organization of the carbon layer stack present in the carbon shells is emphasized in the lattice fringes (Fig. 11) more than in the C_{002} dark field (Figs 10a, b). The stacks are three to four layers thick and the individual BSU are now replaced by continuous layers whose distortions are relatively small. A more or less discontinuous carbon sheet (oriented rim in dark field) takes place around the particle.

3.4.3. Interface

Because of the poor adhesion between the fibre and

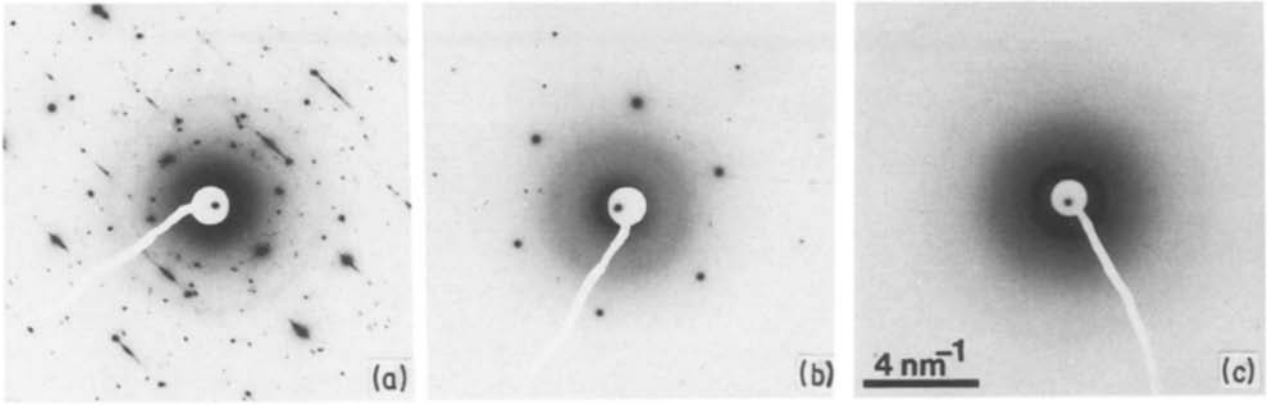

Figure 8 Successive diffraction patterns of a cristobalite particle being irradiated under the electron beam.

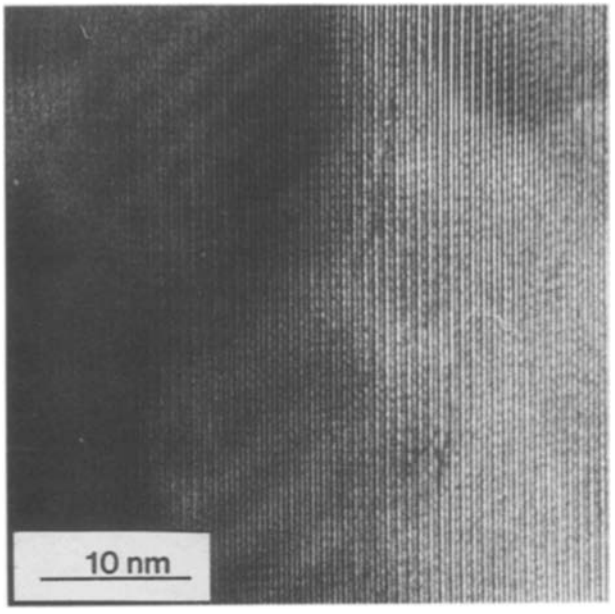

Figure 9 Lattice fringe micrograph of an electron-resistant cristobalite sample, produced from glass crystallization.

cristobalite layer, it is difficult to observe the contact interfaces. Figs 12a and b show C_{002}–SiO_2 and SiC_{111} dark-field images of the interface between the external cristobalite and SiC fibre. Figs 10c and d correspond to the amorphization of the silica crystal in the inset. The comparison between Figs 10a and b and the inset shows that there is no interphase present and that silica is directly in contact with the fibre. The aromatic carbon is present in the same quantities and with the same distribution as in the core of the fibre. On the other hand, the SiC crystals have a different appearance. A double distribution of sizes appears. The larger crystals are few in number and are randomly distributed among a majority of smaller crystals, which look like those of the initial fibre.

4. Discussion and conclusion

This study has shown that among the four SiC fibres studied, only one (NLP 001) is amorphous: the other three are crystalline. The SiC crystal sizes range from 2 nm (NLP 101) to 3 nm (NLP 201) and 7 nm (heat-treated NLP 201). These results are very much in

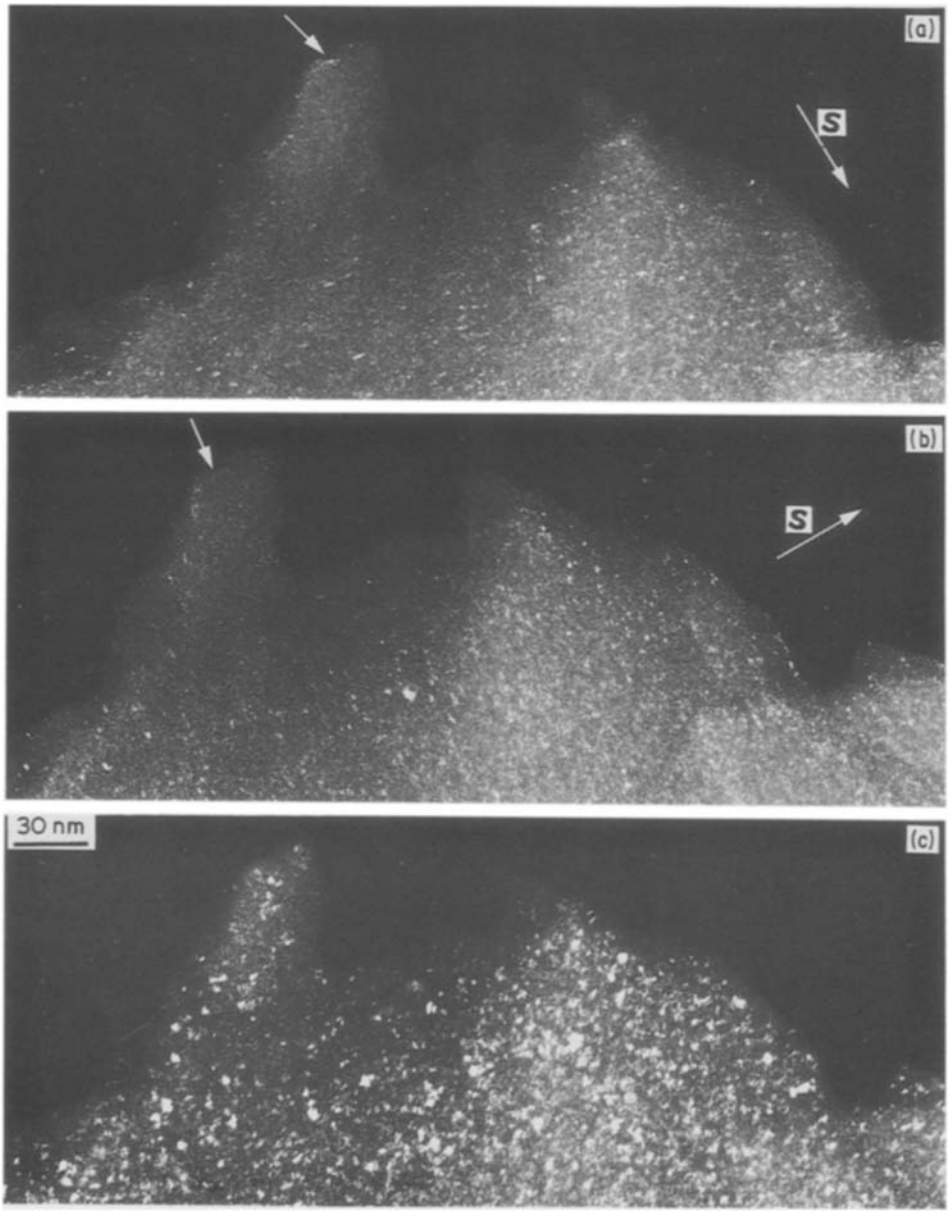

Figure 10 Heat-treated NLP 201 fibre, internal part: (a, b) C_{002} dark fields; (c) SiC_{111} dark field.

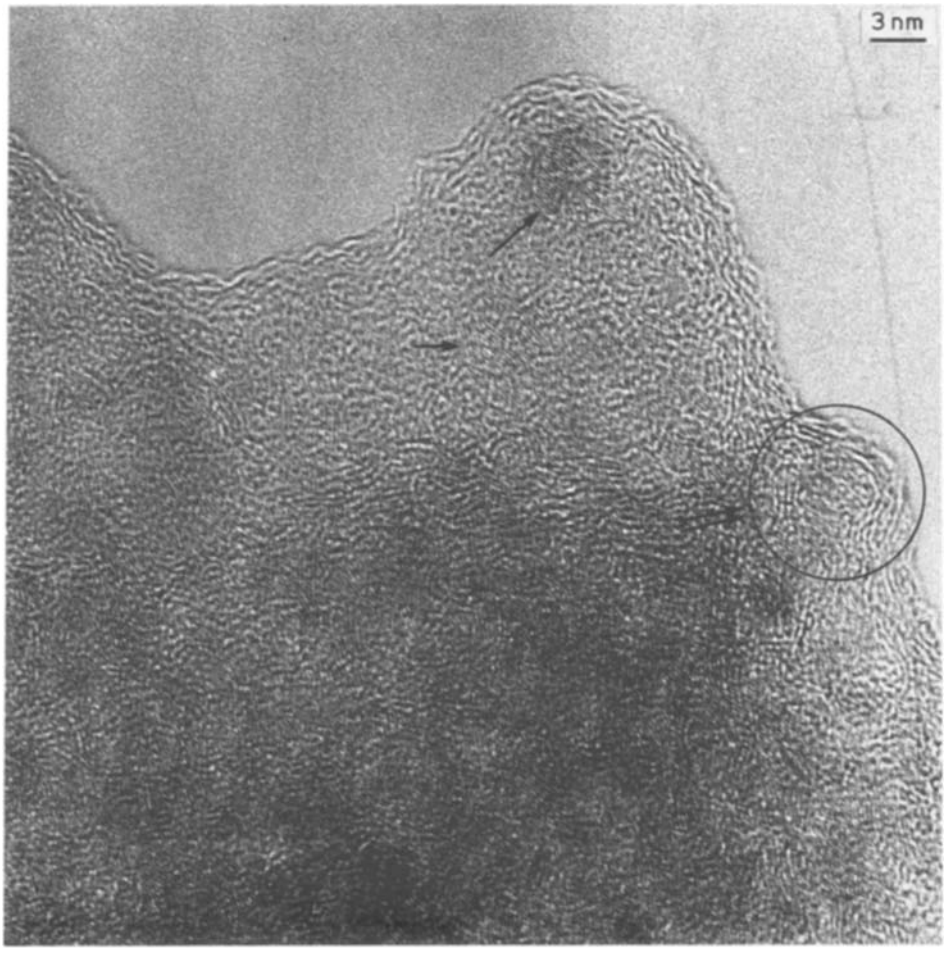

Figure 11 Heat-treated NLP 201 fibre, internal part. Lattice fringes micrograph showing the peculiar arrangement of the SiC crystals and of the carbon nets surrounding them.

agreement with those published recently by Hagege *et al.* [17] which demonstrate a good crystalline organization in the range 1 to 3 nm.

The presence of free carbon, detectable only by the transmission electron microscopy method, has been successfully proved in this paper in all these fibres except NLP 001. Carbon takes the form of aromatic ring structures (basic structural units) which are about 1 nm in size and stacked in groups of two or three. The three-dimensional arrangement is the only parameter which changes from NLP 101 to heat-treated NLP 201. In NLP 101, the basic structural units are single and deposited in a way roughly parallel to the SiC crystals faces. They can only be evinced in C_{002} dark field. In the NLP 201 fibre the basic structural units associate edge to edge in some very distorted layers piled up by three or four, and are visible both in the C_{002} dark field and by means of the lattice fringes technique: they lie parallel to SiC crystals faces. In the heat treated NLP 201 fibre, the basic structural units are replaced by wrinkled continuous layers which are less distorted than in the former sample.

Except for the heat-treated fibres where the data are more obvious (more free carbon, better organized) the three-dimensional arrangement of the carbon BSU is evinced only in C_{002} DF and mainly in the areas where free surfaces oriented edge-on are present, i.e. along the projection of the areas fractured by the microtome knife displacement (microfragments seen in Fig. 1). On the one hand, C_{002} DF avoids blurring of the images by SiC crystal images. On the other hand, edge-on free surfaces favour the superimposition of many edge-on BSU images. Because all fragments are conchoidal in shape they form wedges. The thicker the edge (Fig. 1), the brighter the rim. The thinnest part is almost free of oriented rims: owing to this peculiar feature, the flat deposition of BSU on SiC crystal faces is demonstrated and also the fact that fragmentation occurs preferentially at the level of carbon layers.

The peculiar three-dimensional arrangement of free carbon basic structural units can mainly be shown by a C_{002} dark field where there are free surfaces. The oriented rims can be noticed along fragments looking like those of Fig. 1, especially along the double-arrowed surface. This feature is due to the peculiar shape of the fractured SiC particles during the sectioning operation. The free edges of the broken fragment are limited by the carbon layer stacks, which lie flat on the SiC crystals faces. Because of that preferred orientation, the majority of stacks can be seen on the edge of the fragments in C_{002} dark field, along its thickest part. Indeed, they seem to form a continuous oriented rim in an apparently continuous line. The fragment (see Fig. 1) takes the form of a wedge with an acute conchoidal contour. The thickest edge shows an intense bright rim, whereas the thinnest one is almost invisible.

In the bulk of the particle the basic structural units are randomly distributed and randomly oriented in

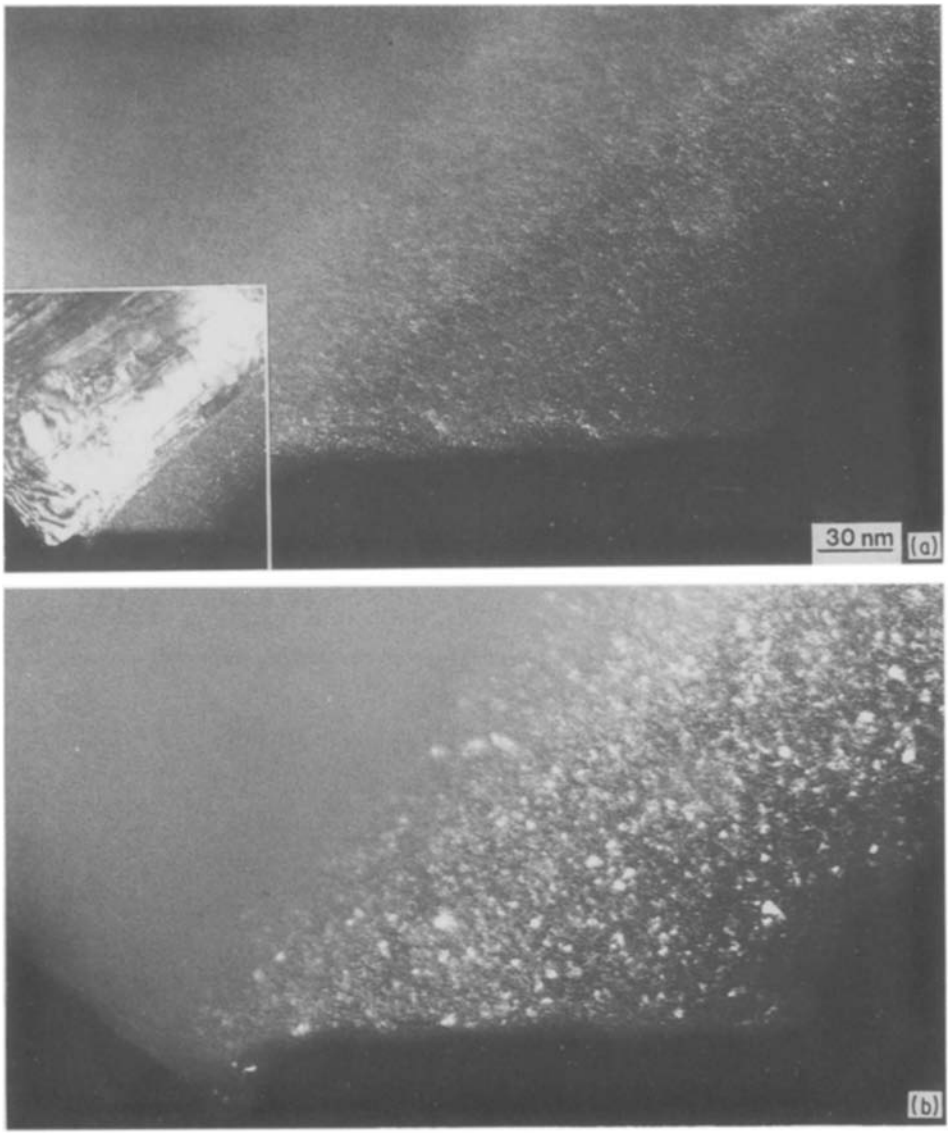

Figure 12 Heat-treated NLP 201 fibre: interface between the silica layer and the SiC fibre. (a) C_{002} dark field. Inset: same view before the amorphization phenomenon. (b) SiC_{111} dark field.

relation to the direction of the incident beam. Hence, they are imaged in C_{002} dark field as individual bright dots. The heat treated NLP 201 fibre is the only sample where the carbon distorted layers occupy enough surface on the SiC crystal faces to be recorded by means of the lattice fringes technique. They appear as short stacks of fringes inside the bulk.

The data obtainable with transmission electron microscopy show at first that when free carbon is detected the fibre is not amorphous. Then, when aromatic turbostratic carbon forms, its basic structural units deposit flat on SiC crystal faces and tend to form nets trapping SiC crystals.

The presence of silica as a localized phase on the surface of the fibre is more questionable. In spite of this, it is assumed to be present because of the results obtained by the ESCA and NMR techniques [17]. It is necessary, however, to distinguish between (SiO_4) tetrahedra connected with ($SiO_{4-x}C_x$) tetrahedra and SiO_2 localized in space. Transmission electron microscopy here is also the only technique capable of recording SiO_2 areas. Thin amorphous silica layers, as thin as 20 nm, were only detected on the NLP 101 fibre. They are assumed, however, to be discontinuous and very rare. Because the observation of the oxidized fibre shows a very low adhesion between silica and SiC fibre, it is obvious that most of the NLP 101 fibre thin silica layer can be chipped off during the embedding operation. The existence of silica on SiC has also been observed by Rahaman and de Jonghe [18] on SiC powders. They succeeded in recording SiC, silica and carbon at the surface of polycrystalline SiC grains. Thin layers of carbon on amorphous silica particles have also been observed in the course of our own experiments.

The silica manifests itself as a 1 μm thick polycrystalline cristobalite layer when the fibre is oxidized. The formation of cracks (Fig. 7a) inside this layer can be explained by the sharp decrease in the volume of cristobalite which occurs at 230° C (beta–alpha transformation). Because of the low adhesion between this layer and the fibre, the layer is easily blown away during mechanical manipulations, and is replaced by the embedding medium when the embedding operation is carried out. This phenomenon is clearly shown in Fig. 7c.

If the oxidization is due to the oxygen diffusion in the fibre, the SiC crystals must exhibit a negative size

gradient from the centre to the exterior of the fibre. The fact that the largest crystals react more slowly to the oxygen than the smallest, explains the double-size distribution. As no increase in the free carbon content is observed, the hypothesis of CO formation is favoured.

Acknowledgement

The Société Européenne de Propulsion is thanked for supplying the samples and for financially supporting this study.

References

1. M. LANCIN, F. ANXIONNAZ, N. SCHUHMACHER, O. DUGNE and P. TREBLIC, *Mat. Res. Symp. Proc.* **78** (1987) 231.
2. M. GUIGON, *Rev. Phys. Appl.* **23** (1988) 229.
3. A. OBERLIN and M. GUIGON, Contract report DRET no. 84087 (1986).
4. T. J. CLARK, M. JAFFE, J. RABE and N. R. LANGLEY, *Ceram. Engng Sci. Proc.* **7** (1986) 901.
5. G. SIMON and A. R. BUNSELL, *J. Mater. Sci.* **19** (1984) 3649.
6. S. YAJIMA, K. OKAMURA, T. MATSUZAWA, Y. HASAGAWA and T. SHISHIDO, *Nature* **279** (1979) 706.
7. N. REID, in "Ultramicrotomy", edited by A. M. Flauert (North Holland, Amsterdam, 1974) p. 296.
8. A. OBERLIN, *Carbon* **17** (1979) 7.
9. *Idem*, in "Kerogen", edited by B. Durand (Technip, Paris, 1980) p. 191.
10. *Idem*, *Carbon* **22** (1984) 521.
11. J. AYACHE, S. BONNAMY, X. BOURRAT, E. BACQUE, M. BIROT and J. DUNNOGUES, *J. Mater. Sci. Lett.* **7** (1988) 885–890.
12. A. OBERLIN, M. OBERLIN and M. MAUBOIS, *Phil. Mag.* **32** (1975) 833.
13. A. OBERLIN, in "Chemistry and Physics of Carbon", Vol. 22, edited by P. J. Walker and P. Thrower (Dekker, New York, 1989).
14. J. N. ROUZAUD and A. OBERLIN, *Thin Solid Films* **105** (1983) 75.
15. Y. MANIETTE, unpublished research, 1987.
16. M. MONTHIOUX, A. OBERLIN and E. BOUILLON, *Compos. Sci. Technol.* in press.
17. R. HAGEGE, P. OLRY, J. COTTERET, M. LARIDJANI, J. DIXMIER, C. LAFFONT, A. M. FLANK, P. LAGARDE, J. L. MIQUEL, H. HOMMEL and A. P. LEGRAND, *J. Mater. Sci.* in press.
18. M. N. RAHAMAN and L. C. de JONGHE, *Amer. Ceram. Soc. Bull.* **66** (1987) 782.

Received 22 July
and accepted 22 November 1988